CFD-modeling for more precise operation of the kraft recovery boiler

MARKUS ENGBLOM, PASI MIIKKULAINEN, ANDERS BRINK, AND MIKKO HUPA

ABSTRACT: During kraft recovery boiler operation, situations can be encountered where the furnace temperature is asymmetric when comparing one side of the furnace to the other (i.e., left vs. right). In this paper, computational fluid dynamics (CFD) modeling is applied to study furnace load and liquor spraying as causes for asymmetric furnace temperatures in a 4450 tons dry solids (TDS)/day kraft recovery boiler. The model predictions are compared against validation measurements. Decrease in furnace load is identified as the main cause of the temperature asymmetry. The simulations also suggest that, at decreased load, relatively small differences in the tilts of individual liquor sprays can increase the temperature asymmetry.

Application: CFD modeling provides mills with a better understanding of kraft recovery furnace combustion.

During kraft recovery boiler operation, situations can be encountered where the furnace temperature is asymmetric when comparing one side of the furnace to the other (i.e., left vs. right). Such situations could be caused by asymmetries in inflows of combustion air and/or black liquor. The air delivery can be asymmetric because of air port positions or differences in air flows through the ports caused by fouling of the ports or differences in damper positions. Liquor guns can be positioned asymmetrically, a different number of liquor guns per wall can be used, or there can be differences between individual liquor sprays because of differences in liquor gun tilts or because of wear or fouling of liquor gun nozzles.

In fact, it would appear that recovery boilers seldom have fully symmetric in-furnace temperature fields and some asymmetry can be expected. Slight asymmetries need not lead to operational problems. However, potential drawbacks associated with increasingly asymmetric furnace temperatures could include decreased steam production due to the deviation from the design temperature field as well as increased risk for superheater corrosion due to locally high flue gas temperature. The temperature asymmetry can also be expected to be connected with an increase in carbon monoxide emission due to improper mixing of fuel and combustion air, as well as an uneven carryover load when comparing the furnace's left and right sides. Counteracting the increased carbon monoxide by increasing the flue gas excess oxygen can in turn increase the boiler NOx emissions.

Better understanding of the causes of asymmetric furnace temperatures could potentially be used for more precise operation of the kraft recovery boiler in order to reduce gaseous emissions and to increase boiler efficiency and availability. This paper focuses on asymmetric furnace temperatures observed during a measurement campaign of a 4450 tons dry solids (TDS)/day kraft recovery boiler. Computational fluid dynamics (CFD) modeling is carried out to study the impacts of furnace load and liquor spraying on in-furnace temperatures. Model predictions are compared against validation measurements and process data.

KRAFT RECOVERY BOILER MEASUREMENT CAMPAIGN

A comprehensive measurement campaign of a 4450 TDS/day kraft recovery boiler was carried out in order to obtain in-furnace validation data for CFD modeling. During the campaign, the furnace was operated at 70% load. Measurements included flue gas temperatures and gas species [1,2]. **Figure 1** presents measured temperatures and gas species. To complement the below-bullnose measurements, process data was collected as shown in Fig. 1 and **Fig. 2**. In general, the gas temperatures on the

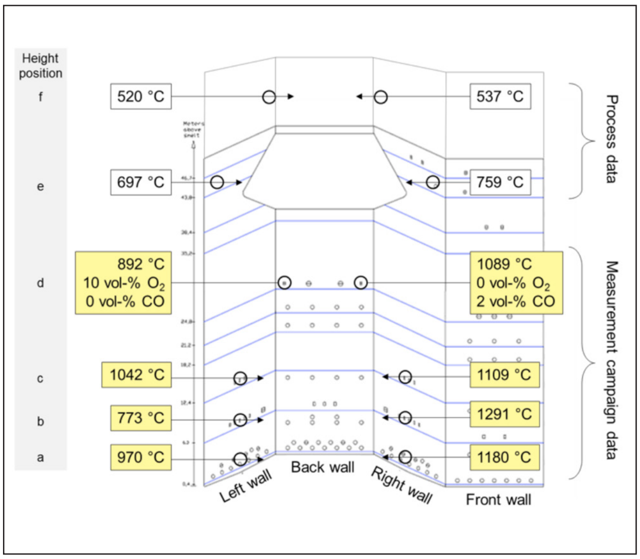

1. In-furnace temperatures and gas species during measurement campaign [1,2]. The process data on flue gas temperatures corresponds to measurement points 1 and 3 in Fig. 2.

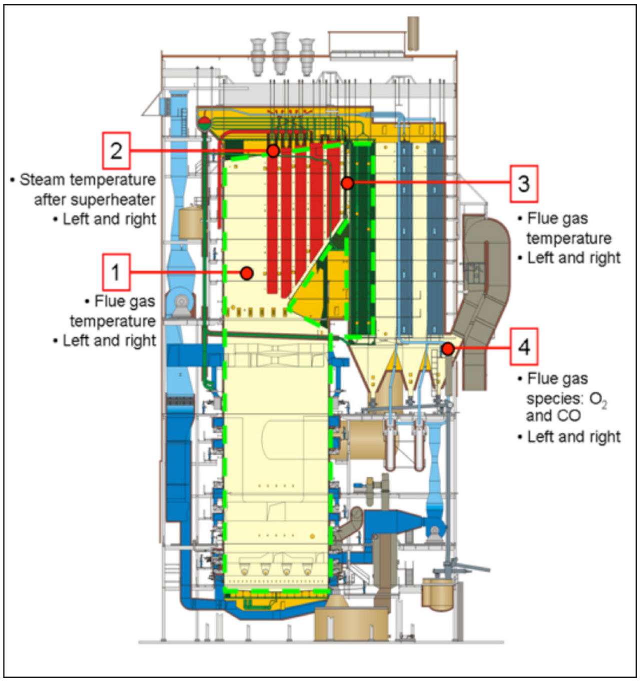

2. Measurement locations and type of process data collected from the upper part of the recovery boiler. The green line shows the modeled region of the furnace.

furnace right side were higher than on the left side. In-furnace concentrations of oxygen and carbon monoxide were also measured through the furnace back wall, above the tertiary air level [2]. The higher gas temperature on the right side of the furnace correlated with reducing conditions, whereas the lower temperatures on the left side correlated with oxidizing conditions. This indicates that the lower temperature on the furnace left side was due to dilution of the furnace gas with excess combustion air.

Effort was also put into obtaining good input data for modeling. Air ports were maintained clean and their damper positions were noted. In addition, air port gas velocities were measured when possible, using a specially designed pitot tube. No clear differences in air port gas velocities were observed when comparing corresponding ports on the left and right sides of the furnace. However, the furnace has some asymmetry when considering the placements of air ports. Not all corresponding air ports on the left and right sides are positioned at equal distances from the centerline.

The liquor and liquor spraying were also characterized to considerable detail. The liquor originated from pulping of a 50/50 mixture of hardwood and softwood. Standard fuel analysis of the as-fired liquor was carried out. In addition, experiments in a laboratory furnace were carried out using single droplets to determine liquor swelling. Droplet swelling was 3.6, taken as the ratio between the maximum swollen diameter and the initial diameter. The as-fired liquor had a solids content of 82.7%, temperature of 140°C, and density of 1466 kg/m^3 [3]. The liquor spray was operated in the flashing regime, with the liquor temperature 20°C above its boiling point. **Figure 3** presents liquor gun positions during the campaign. Black liquor was introduced using six liquor guns altogether, with three guns positioned on each side wall. Figure 3 also shows the liquor gun barrel tilts during the campaign. On average the liquor guns on the right side wall were tilted more toward the char bed as compared to the guns on the left side wall.

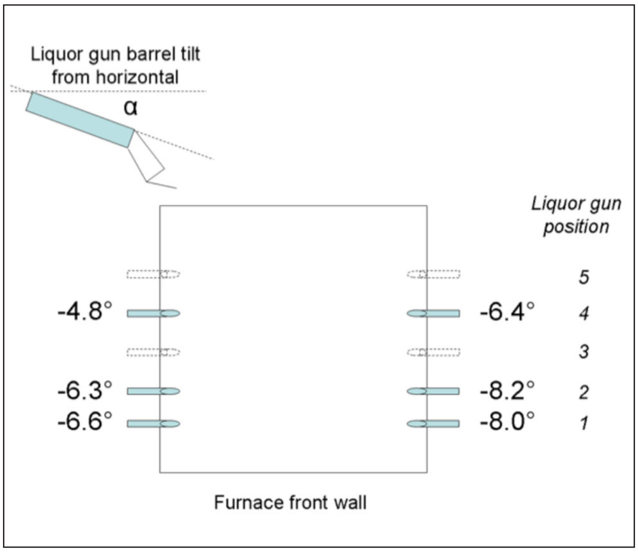

3. Liquor gun positions and liquor gun barrel tilts measured using a digital spirit level. There are five liquor gun openings on each side wall. During the measurement campaign, the furnace was operated with three liquor guns on each wall.

Figure 4 presents infrared (IR) images of the spray during the campaign. Spray opening angles were estimated from the figures as a horizontal opening angle of 140° and a vertical opening angle of 14°. The average spray tilt was estimated as -3° from horizontal.

The spray was also characterized using procedures based on image analysis (e.g., [4]). **Figure 5** presents example images from which droplet data were determined [3]. The droplets were estimated to have a mass-median diameter of 12.7 mm and aspect ratios (width-to-height ratios) ranging from 1.33 to 1.71, with an average aspect ratio of 1.37. The droplet aspect ratio was observed to increase with drop size, i.e., larger droplets were less spherical. In Fig. 5, the images show some droplets to be transparent, indicating that they are hollow and suggesting that their density is low. Droplet velocities as a function of distance from the liquor nozzle were also determined (Fig. 7).

SIMULATION CASES AND SIMULATION SETUP

Simulations were carried out using the Åbo Akademi Furnace Model, which uses commercial CFD software as a platform, and to which application specific sub-models have been developed for droplet combustion and char bed combustion [5,6]. The purpose of the simulations was to study boiler load and liquor spraying as causes for asymmetric furnace

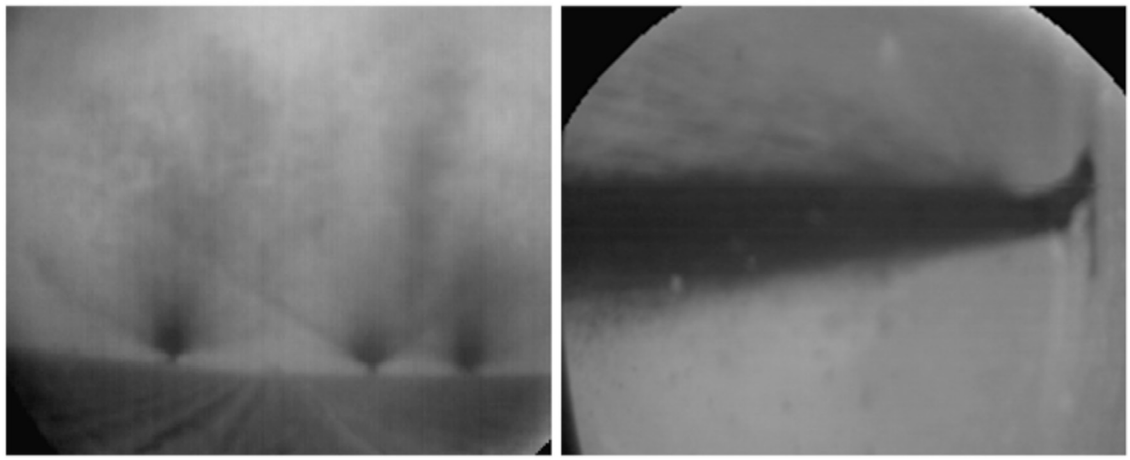

4. Infrared (IR) images of the liquor sprays during the measurement campaign, as seen from above (left) and from the side (right).

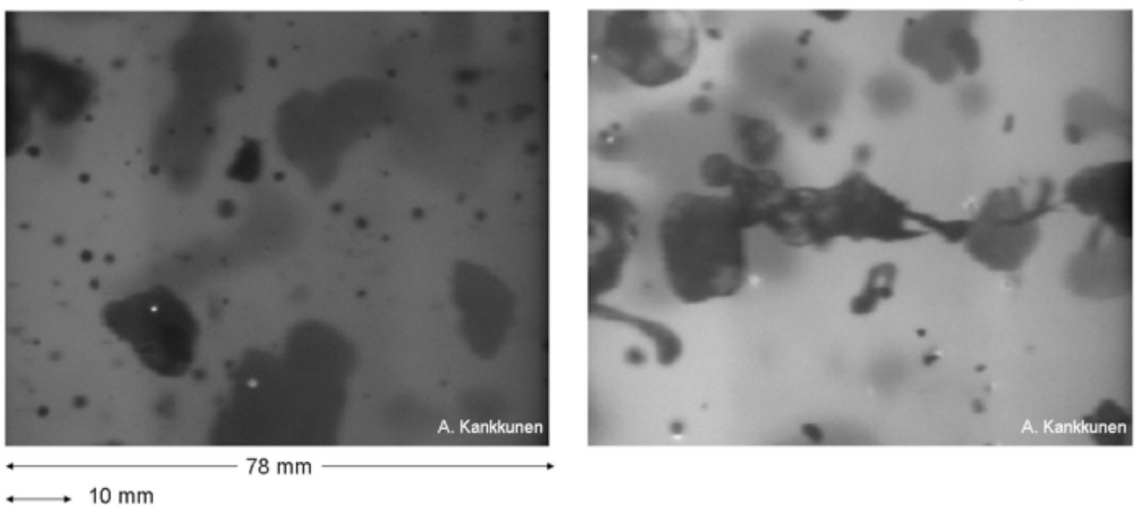

5. Images of liquor droplets at a distance of 2.3 meters from the liquor gun nozzle.

temperatures. Two boiler loads and two spray configurations were combined into four simulation cases (**Fig. 6**). The simulated region of the furnace is indicated in Fig. 2 by the green line.

The boiler loads considered were 90% and 70% of the rated capacity. The 70% load corresponds to the situation during the measurement campaign. For each load, the distribution of combustion air to the different air levels was representative of actual operation. The air distribution into primary, secondary, and tertiary was 23%, 43%, 35% and 24%, 45%, 31% for loads 90% and 70%, respectively. The air velocity at air ports was determined considering the actual open area due to damper positions. Air velocities and mass flows with equal magnitude were used on corresponding air ports on the left and right sides of the furnace. A different number of liquor guns was used for the two loads, consistent with actual operations. For loads 90% and 70%, 8 and 6 liquor guns were used, respectively. Figure 6 presents liquor gun positions in the simulations.

Figure 6 also presents the spray tilts used in the simulations. In the "Common spray tilt" configuration, all sprays have the same tilt. The value -3° was used, as estimated from the images of the spray during the measurement campaign (Fig. 4). In the "Individual spray tilts" configuration, each liquor gun was assigned an individual spray tilt. The liquor gun on the left wall in position 4 was assumed to have a spray tilt of -3°. In the case of 70% load, the tilts of the remaining liquor sprays were set considering the differences in barrel tilts measured during the campaign (Fig. 3).

For the 90% load, there was no knowledge of the actual barrel tilts or spray tilts. When using individual spray tilts, the tilts of the liquor guns in positions 1, 2 and 4 were assumed

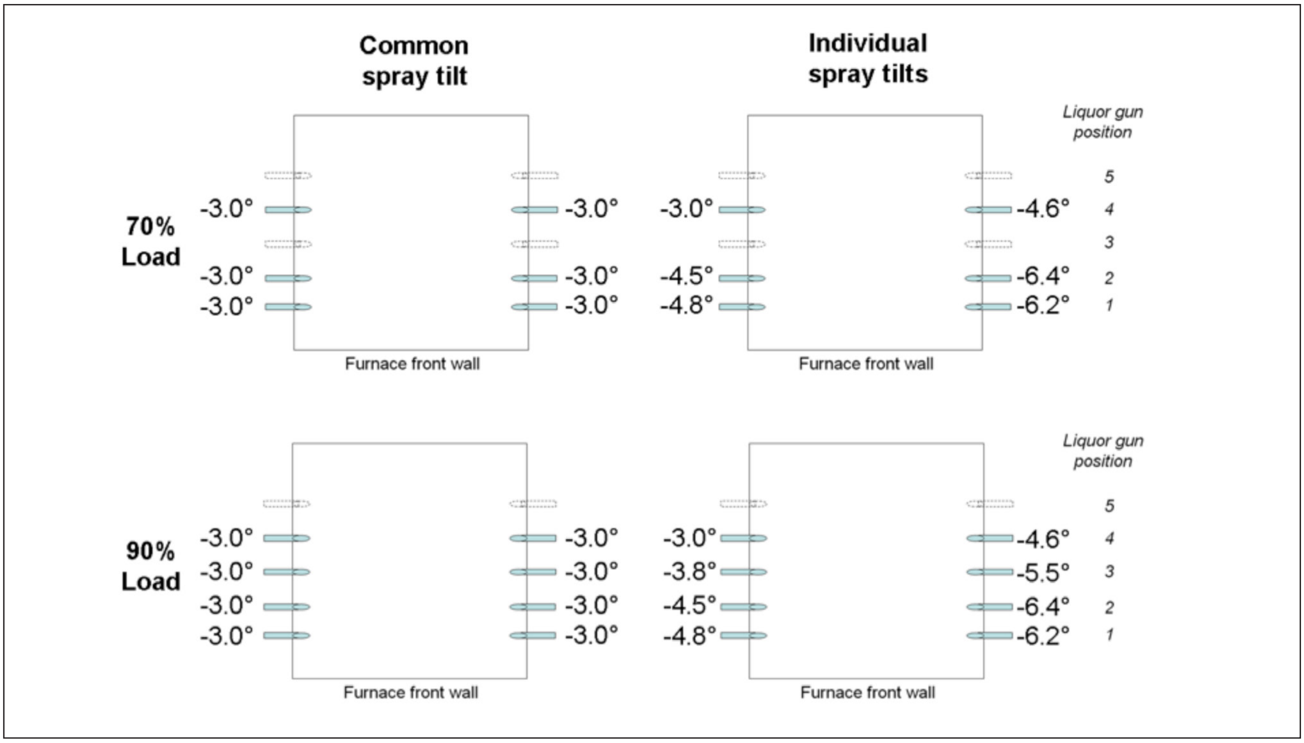

6. Placement of liquor guns and spray tilts (degrees from horizontal) in simulation cases.

to be the same as with the 70% load. For the additional sprays, corresponding to liquor guns in position 3, the spray tilt was assumed to be the average of that of the neighbor sprays. All liquor sprays were modeled as having horizontal and vertical opening angles of 140° and 14°, respectively, as estimated from the images of the spray during the measurement campaign (Fig. 4). The opening angles define the boundaries within which droplets are injected. The liquor mass flow distribution and velocity distribution inside the opening angles are modeled considering experimental data [7]. The mass flow is greatest in the center of the spray and the velocity is constant over the opening angles. More details of the spray model can be found in [8].

The droplet formation process during liquor spraying is not included in the model. Instead, the model input consists of a set of droplet boundary conditions, defining the initial states of the droplets. In addition to the spray characteristics described above, droplet boundary conditions include droplet size distribution and density. Additionally, droplet swelling is a model input.

Droplet size distribution was modeled using a Rosin-Rammler function, with average droplet diameter 14.5 mm and spread parameter 2.75 [3]. Images from the liquor spray during the measurement campaign included transparent droplets, suggesting low density (Figure 5). The initial density used in the droplet model was determined such that it resulted in simulated droplets having velocities consistent with in-furnace data. The initial droplet density used in the four furnace simulation cases was 138 kg/m^3. **Figure 7** presents droplet velocities as a function of distance from the liquor gun nozzle. Experimental data is given for large (>10 mm) and small (<2 mm) droplets.

The procedure for determination of the initial droplet density involved as a first step a preliminary furnace simulation, followed by droplet trajectory calculations using different initial droplet densities. After determining 138 kg/m^3 as a suitable initial droplet density, that density was then used in the four furnace simulation cases. Figure 7 shows the effect of initial droplet density on predicted droplet velocities for three initial densities, including the one used in the furnace simulations (Case 2).

In Fig. 7, Case 1 is a first assumption of liquor swelling during flashing based on observations under laboratory conditions. In laboratory burning, the droplet diameter increases typically by a factor of 1.5 during heat-up to boiling point, followed by liquor-specific further swelling [9]. In Case 1, it is assumed that the swelling by the factor 1.5 takes place during the droplet formation process, resulting in an initial droplet density of 434 kg/m^3. In Case 1, it is further assumed that the maximum swelling, at end of pyrolysis, is equal to the one determined for this liquor under laboratory conditions.

In Fig. 7, Case 2, it is assumed that swelling by a factor of 2.2 takes place during the droplet formation process. In lack of experimental data on liquor swelling under furnace conditions, the maximum swelling is assumed equal to the one determined for this liquor under laboratory conditions. Case 2 was considered to give reasonable agreement with experimental data, particularly for droplets with an initial diameter of ≥10 mm. In the furnace simulations, these large droplets represent most of the liquor spray mass flow.

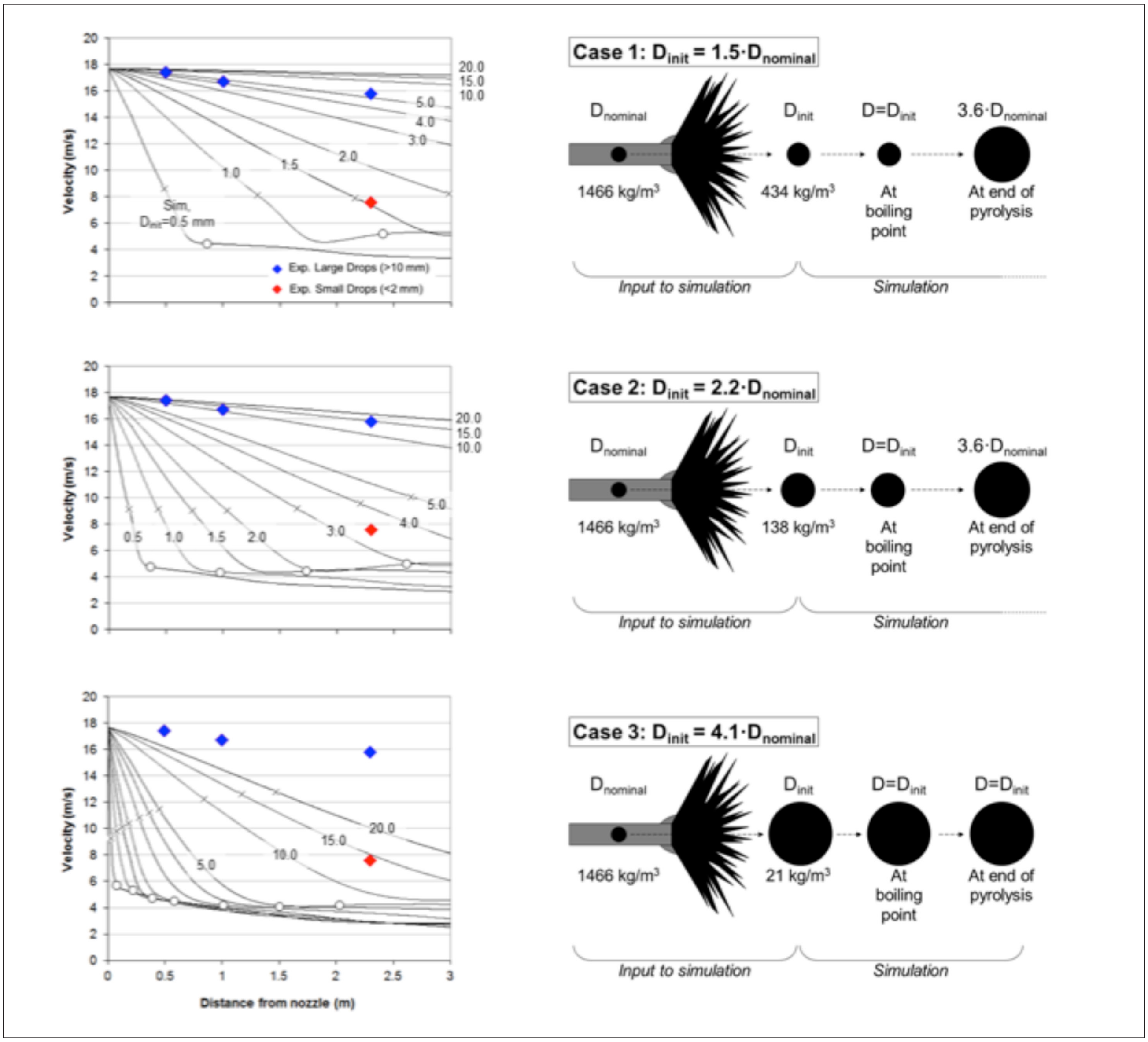

7. Experimental [3] and simulated droplet velocities as a function of the distance from the liquor nozzle. Droplets with initial diameters of 0.5-20.0 mm were simulated using three different initial densities (Cases 1, 2, and 3). $D_{nominal}$ refers to the diameter of a drop of liquor inside the liquor gun. D_{init} is the initial droplet diameter given as input to the droplet model. The markers "x" and "o" indicate onset and end of pyrolysis, respectively.

In Fig. 7, Case 3 represents the theoretical extreme situation of maximum swelling due to liquor flashing. This case assumes that the energy associated with the liquor excess temperature (20°C) produces steam that remains inside the liquor droplet. This was calculated to result in an increase in the droplet diameter by a factor of 4.1 during the droplet formation process. Further swelling was assumed not to occur during pyrolysis.

The initial droplet density has a considerable effect on droplet burning. This is indicated in Fig. 7 by the onset and end of pyrolysis. Furnace simulations were carried out (but not reported here in detail) using the three initial droplet densities of Fig. 7. A decrease in the initial density resulted in more in-flight combustion and less char carbon reaching the furnace walls and char bed. The initial droplet density appears to be an important input when modeling liquor spraying in the flashing regime.

In determination of the initial droplet density, the droplets were assumed to be spherical. This is in contrast to the non-spherical droplets observed during the measurement campaign. While droplet shape affects the predicted droplet trajectory and burning, the effect is relative small for aspect ratio less than 2 [10]. Trajectory calculations were performed to test the impact of non-spherical droplets. Assuming an ellipsoid with an aspect ratio of 1.71, a droplet velocity behavior similar to that in Case 2 was obtained when the initial swelling number was 2.0. The initial droplet density had a greater effect on predictions when considering the range of densities studied.

SIMULATION RESULTS AND DISCUSSION

In this section, the simulation results are discussed by first considering the impact of furnace load. The predictions at 90% and 70% load are compared with process data from the upper part of the boiler. Second, predictions at 70% load are compared against in-furnace measurements, and the impact of liquor spraying is discussed.

Furnace load

Figure 8 presents simulated furnace temperatures. In all simulation cases, the upper furnace temperature on the right side is greater than on the left side. Furnace load is seen to have a considerable effect on the temperature asymmetry. The asymmetry is greater in the case of 70% load as compared to the 90% load. With the 70% load, the flue gas flow is smaller, and the greater asymmetry is due to the flue gas flow being less uniform over the furnace cross section (**Fig. 9**).

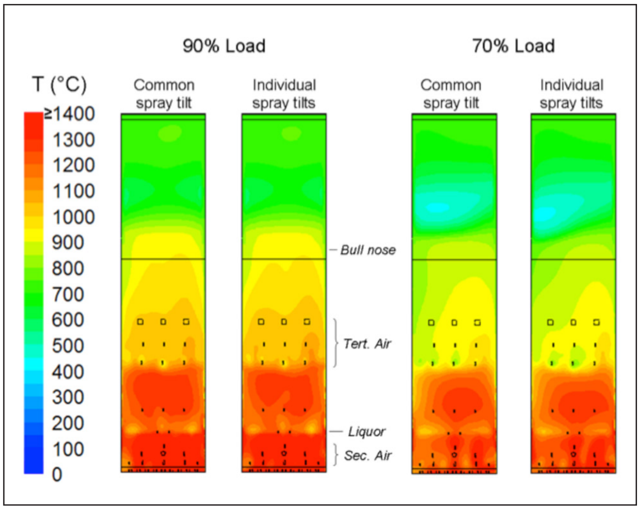

8. Simulated temperatures on the furnace center plane, as seen through the furnace front wall.

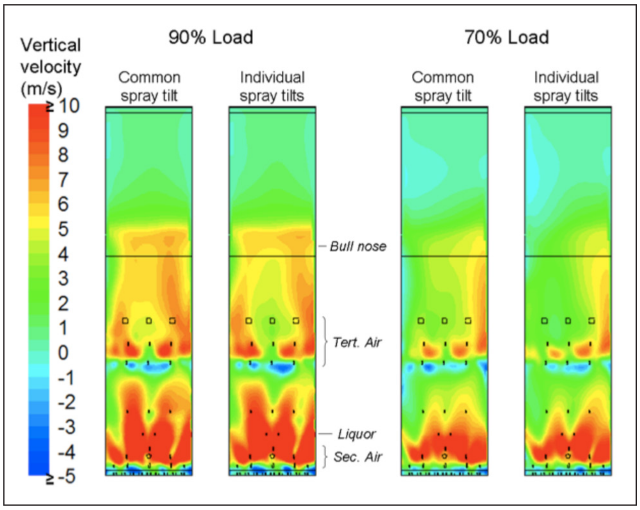

9. Simulated vertical gas velocity (positive is upward direction) on the furnace center plane, as seen through the furnace front wall.

Figure 10 presents process data from the upper part of the boiler for loads 90% and 70%. The numbers given are one-day averages. The data shows that the temperature difference decreases in magnitude along the flue gas path and that the temperature difference of steam from the first superheater is relatively small irrespective of load. The data also indicates greater asymmetry in case of 70% load as compared to 90% load. In the simulations, the temperature difference of the flue gas in the region before the superheaters was about 100°C and about 10°C for loads 70% and 90%, respectively. It appears that the model correctly predicts the trends, but not the absolute values. However, in the case of 70% load the predicted temperature difference in this region depends relatively much on the exact location considered.

The simulations are steady-state predictions, representing time-averaged situations. However, the process data shows the real process to typically exhibit time-dependent fluctuations. Such fluctuations cannot be predicted with the current model. **Figures 11** and **12** present time series of the differences in flue gas temperature before the first superheater and the oxygen concentration before the electrostatic precipitator (ESP), respectively. The flue gas data in Fig. 11 shows that there can be considerable fluctuations with time, and that momentarily the temperature difference with 90% load was of similar or greater magnitude as compared to that with 70% load. The oxygen data in Fig. 12 is from the same time intervals as the temperature data in Fig. 11. The magnitude of the oxygen concentration difference is consistently greater in the case of 70% load as compared to 90% load. The discrepancy between the temperature and oxygen concentration data indicates greater time-dependent fluctuations in flue gas flow before the superheaters than after them.

Modeling vs. measurements

Brink et al. report the experimental temperatures not to be point measurements, but weighted line averages [1]. Brink et al. estimate the temperatures to represent conditions 2 to 3 meters from the furnace inner wall. The predicted temperature field has considerable temperature gradients in some locations. This makes the determination of representative predicted temperatures less straighforward. However, an attempt was made by extracting volume-weighted average temperatures from the simulation results. The temperatures were calculated by considering a sphere with a centroid located 2.5 m from the furnace wall and having a diameter of 0.5 m. **Figure 13** presents simulated volume-averaged temperatures and measured temperatures at 70% load.

In Fig. 13, simulated and measured temperatures are seen in general to be of similar magnitude. The simulated temperatures are to some extent affected by the model predicting overall carbon accumulation in the furnace,

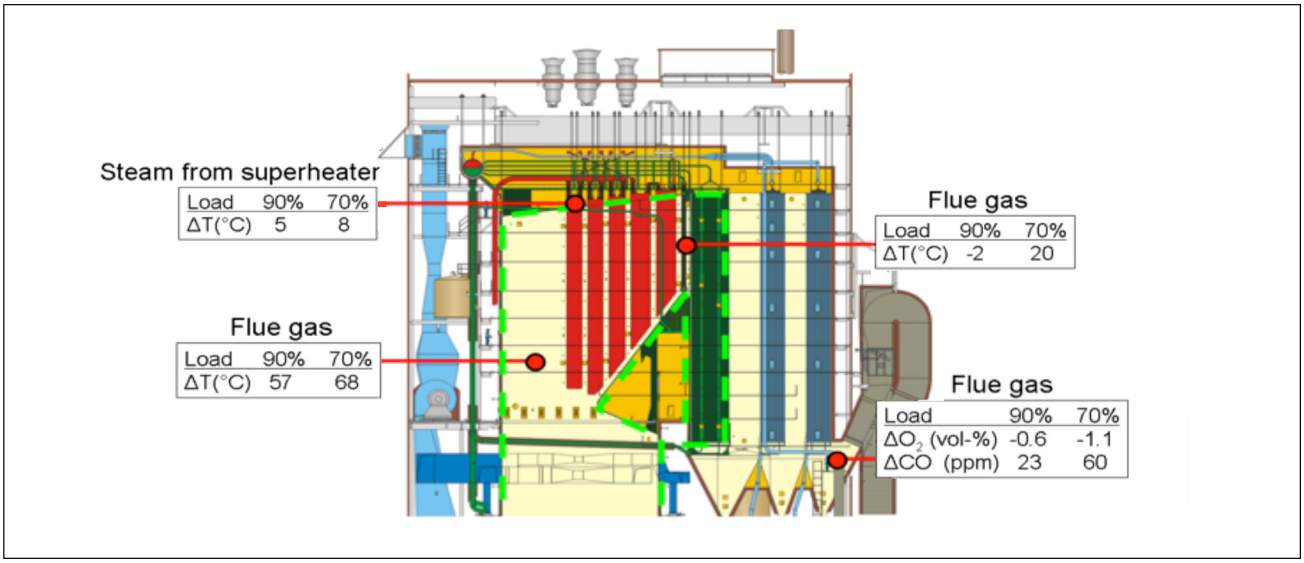

10. Time-averaged differences (Δ = right– left) of temperature and of concentrations of oxygen and carbon monoxide, based on one-day averaged process data for loads of 90% and 70%.

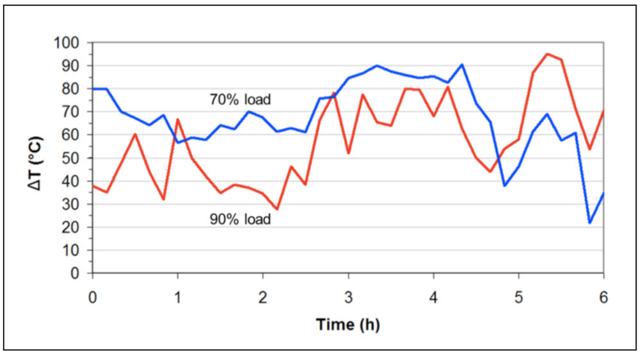

11. Flue gas temperature difference (right side – left side) at boiler loads of 90% and 70%, based on process data on flue gas temperatures above the bullnose before the first superheater.

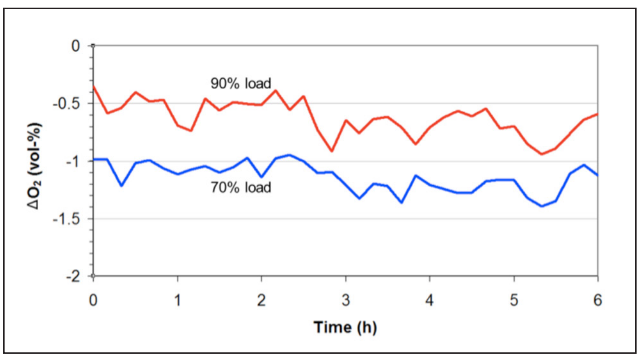

12. Oxygen concentration difference (right side – left side) at boiler loads of 90% and 70%, based on process data on oxygen concentration before the ESP.

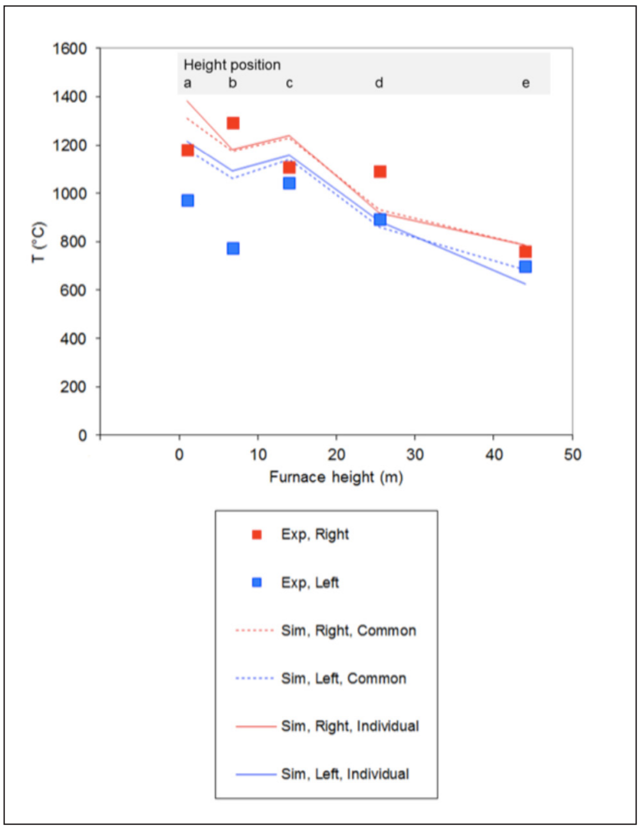

13. Measured and modeled temperatures at 70% boiler load. Measured temperatures are estimated to represent in-furnace conditions of 2 -3 m from the furnace inner wall [1]. The measured temperatures correspond to temperatures in Fig. 1, excluding the temperature after the superheaters. Modeled temperatures are from simulations using common spray tilts and individual spray tilts, and are volume-weighted average temperatures within a sphere with centroid 2.5 m from the furnace wall and a diameter of 0.5 m.

resulting in greater overall excess oxygen (5 vol-% O_2) and lower adiabatic flame temperature as compared to that in the case of the overall stoichiometry in the real process (3 vol-% excess O_2). The magnitude of the effect is location-specific, depending on the local predicted conditions. In Fig. 13, at two height positions b and d, the predicted temperature differences between the left and right sides are considerably smaller than the experimental ones. These positions correspond to the locations of liquor spraying and furnace back wall above tertiary air (Fig. 1). However, in Fig. 13, the predicted temperatures are higher on the furnace right side as compared to the ones on the left side. This is consistent with the trend of the experimental temperatures.

In Fig. 13, liquor spraying is seen to affect predicted temperatures to some extent. When changing from common spray tilt angles to individual ones, the temperature difference between left and right side is most increased at height positions a and e. These positions correspond to the locations above the char bed and above the bull nose before the first superheater (Fig. 1). In Figs. 8 and 9, at 70% load, an increase in temperature and gas flow asymmetry due to individual spray tilts can also be seen. The simulations suggest that liquor spraying could have contributed to the temperature asymmetry observed during the measurement campaign. No experimental data on the impact of liquor spray tilt was available to confirm the predictions. In Fig. 8, spray tilts are seen to have less impact on temperature asymmetry at 90% load than at 70% load. It seems reasonable to expect that at lower furnace load, even small asymmetries in inflows of liquor or combustion air can be sufficient to trigger or increase the furnace temperature asymmetry.

SUMMARY AND CONCLUSIONS

CFD-based modeling was carried out to investigate furnace load and liquor spraying as causes for asymmetric furnace temperatures in a 4450 TDS/day kraft recovery boiler. Simulation results were compared against validation measurements. The modeling proved to be a useful tool for investigating the possible causes of in-furnace phenomena. The following conclusions are made:

- Some extent of asymmetric in-furnace gas flows and temperatures can be expected in most cases as a result of asymmetries in inflows of combustion air and/or black liquor, caused by, e.g., air port positions, fouling of air ports, damper positions, liquor gun positions, number of liquor guns, gun tilts, and wear or fouling of liquor gun nozzles.

- A decrease in furnace load can be expected to lead to or increase the temperature asymmetry. For boiler operation, the propensity for asymmetric in-furnace conditions due to a decrease in boiler load can be inherent to the situation and may be challenging to counteract completely.

- With decreasing load, relatively small differences in liquor spray tilts can affect the extent of the temperature asymmetry. For boiler operation, it can be beneficial to also consider liquor spraying if measures are sought to abate temperature asymmetry.

- For CFD modeling, accurate model input concerning liquor spraying is important for simulation accuracy. Proper input for air introduction is also essential. Even minor differences in input symmetry might cause the asymmetric behavior of a simulated boiler. **TJ**

ABOUT THE AUTHORS

We chose this research topic because kraft recovery furnace combustion processes are complex. Modeling can give new insight into and better understanding of these processes.

In this study, we had unique in-furnace measurements, and we were interested in applying CFD modeling to see how well the predictions would agree with these measurements, and if we could identify the cause of the temperature asymmetry. The novelty for us was that this was a first effort at large scale model validation.

Setting up the furnace model was the most challenging aspect of this research because we wanted to be sure we were modeling the situation during the measurement campaign. Having representative boundary conditions was important.

It was interesting to see the agreement between measurements and modeling. We hope the findings can be used in boiler operations at mills. In the future, there is a need for more comprehensive validation of CFD-based furnace models.

Engblom

Brink

Hupa

Miikkulainen

Engblom is a researcher, Brink is associate professor, and Hupa is professor at Åbo Akademi University in Turku, Finland. Miikkulainen (D.Sc.) is product manager, recovery boilers, for Andritz Pulp and Paper's Recovery and Power Division, Andritz Oy, Kotka, Finland. Email Engblom at markus.engblom@abo.fi.

ACKNOWLEDGEMENTS

This work has been carried out within the projects ChemCom 2.0 (2008-2010) and FUSEC (2011-2014) as part of the activities of the Åbo Akademi Process Chemistry Centre. Support from the Academy of Finland in their Centres of Excellence Program, the National Technology Agency of Finland and industrial partners Andritz Oy, Metso Power Oy, Oy Metsä-Botnia Ab, Foster Wheeler Energia Oy, UPM-Kymmene Oyj, Clyde Bergemann GmbH, International Paper Inc. and Top Analytica Oy Ab is gratefully acknowledged

Juha Kyttälä, VTT Technical Research Centre of Finland, is acknowledged for providing the calculation grid and boundary conditions for the CFD simulations.

REFERENCES

1. Brink, A., Laurén, T., Hupa, M., et al., *TAPPI J.* 9(7): 7(2010).
2. Vainio, E., Brink, A., DeMartini, N., et al., *J. Pulp Pap. Sci.* 36(3-4): 135(2010).
3. Kankkunen, A.K., Miikkulainen, P.H., and Fogelholm, C.-J., *Int. Chem. Recovery Conf.*, TAPPI PRESS, Atlanta, GA, USA, 2010, vol. 2, p. 114.
4. Kankkunen, A., personal communication.
5. Mueller, C., Eklund, K., Forssén, M., et al., *Int. Chem. Recovery Conf.*, TAPPI PRESS, Atlanta, 2004, p. 979.
6. Bergroth, N., Engblom, M., Mueller, C., et al., *TAPPI J.* 9(2): 6(2010).
7. Miikkulainen, P., Järvinen, M., and Kankkunen, A., *Pulp Pap. Can.* 103(9): 34(2002).
8. Li, B., Brink, A., Engblom, M., et al., C-J., "Spray models for CFD of black liquor recovery furnaces," *IFRF Members Conf., 15th*, International Flame Research Foundation, Livorno, Italy, 2007.
9. Hupa, M., Solin, P., and Hyöty, P., *J. Pulp Pap. Sci.* 13(2): 67(1987).
10. Järvinen, M., Kankkunen, A.P., Miikkulainen, P.H., et al., *Int. Chem. Recovery Conf.*, TAPPI PRESS, Atlanta, 2004, p. 81.